A&A 476, 935–950 (2007)
DOI: 10.1051/0004-6361:20077706

Astronomy & Astrophysics

First stars

VIII. Enrichment of the neutron-capture elements in the early Galaxy⋆

P. François[8,1], E. Depagne[1,10], V. Hill[1], M. Spite[1], F. Spite[1], B. Plez[2], T. C. Beers[3], J. Andersen[5,9], G. James[8,1], B. Barbuy[4], R. Cayrel[1], P. Bonifacio[1,6], P. Molaro[6], B. Nordström[5], and F. Primas[7]

[1] GEPI, Observatoire de Paris-Meudon, CNRS, Univ. de Paris Diderot, Place Jules Janssen, 92190 Meudon, France
e-mail: Patrick.Francois@obspm.fr
[2] GRAAL, Université de Montpellier II, 34095 Montpellier Cedex 05, France
[3] Dept. of Physics & Astronomy, CSCE: Center for the Study of Cosmic Evolution, and JINA: Joint Institute for Nuclear Astrophysics, Michigan State University, E. Lansing, MI 48824, USA
[4] IAG, Universidade de São Paulo, Departamento de Astronomia, CP 3386, 01060-970 São Paulo, Brazil
[5] The Niels Bohr Institute, Astronomy Group, Juliane Maries Vej 30, 2100 Copenhagen, Denmark
[6] Istituto Nazionale di Astrofisica - Osservatorio Astronomico di Trieste, via G.B. Tiepolo 11, 34131 Trieste, Italy
[7] European Southern Observatory (ESO), Karl-Schwarschild-Str. 2, 85749 Garching b. München, Germany
[8] European Southern Observatory (ESO), Alonso de Cordova 3107, Vitacura, Casilla 19001, Santiago 19, Chile
[9] Nordic Optical Telescope, Apartado 474, 38700 Santa Cruz de La Palma, Spain
[10] Las Cumbres Observatory, Santa Barbara, California, USA

Received 24 April 2007 / Accepted 18 September 2007

ABSTRACT

Context. Extremely metal-poor (EMP) stars in the halo of the Galaxy are sensitive probes of the production of the first heavy elements and the efficiency of mixing in the early interstellar medium. The heaviest measurable elements in such stars are our main guides to understanding the nature and astrophysical site(s) of early neutron-capture nucleosynthesis.
Aims. Our aim is to measure accurate, homogeneous neutron-capture element abundances for the sample of 32 EMP giant stars studied earlier in this series, including 22 stars with [Fe/H] < -3.0.
Methods. Based on high-resolution, high S/N spectra from the ESO VLT/UVES, 1D, LTE model atmospheres, and synthetic spectrum fits, we determine abundances or upper limits for the 16 elements Sr, Y, Zr, Ba, La, Ce, Pr, Nd, Sm, Eu, Gd, Dy, Ho, Er, Tm, and Yb in all stars.
Results. As found earlier, [Sr/Fe], [Y/Fe], [Zr/Fe] and [Ba/Fe] are below Solar in the EMP stars, with very large scatter. However, we find a tight anti-correlation of [Sr/Ba], [Y/Ba], and [Zr/Ba] with [Ba/H] for $-4.5 <$ [Ba/H] < -2.5, also when subtracting the contribution of the main *r*-process as measured by [Ba/H]. Spectra of even higher S/N ratio are needed to confirm and extend these results below [Fe/H] $\simeq -3.5$. The huge, well-characterised scatter of the [n-capture/Fe] ratios in our EMP stars is in stark contrast to the negligible dispersion in the [α/Fe] and [Fe-peak/Fe] ratios for the same stars found in Paper V.
Conclusions. These results demonstrate that a second ("weak" or LEPP) *r*-process dominates the production of the lighter neutron-capture elements for [Ba/H] < -2.5. The combination of very consistent [α/Fe] and erratic [n-capture/Fe] ratios indicates that inhomogeneous models for the early evolution of the halo are needed. Our accurate data provide strong constraints on future models of the production and mixing of the heavy elements in the early Galaxy.

Key words. stars: abundances – stars: Population II – Galaxy: abundances – Galaxy: halo – nuclear reactions, nucleosynthesis, abundances

1. Introduction

In cold dark matter models for hierarchical galaxy formation, the very first generation of metal-free (Population III) stars are thought to be born in sub-galactic fragments of mass $M > 5 \times 10^5\ M_\odot$ (Fuller & Couchman 2000; Yoshida et al. 2003; Madau et al. 2004). Recent models of primordial star formation (Abel et al. 2000; Bromm 2005) suggest that these stars were very massive ($M > 100\ M_\odot$), although substantial uncertainties remain.

It is likely that none of these stars survives in the Galaxy today. However, this first generation of stars left imprints of its nucleosynthetic history in the elemental abundance patterns of the most metal-poor lower-mass stars that we can observe at present. Detailed chemical analyses of the most metal-poor stars can therefore provide insight into the synthesis of the first heavy elements and how efficiently they were mixed and incorporated in later stellar generations – i.e. how large spiral galaxies such as our own were first assembled.

In Paper V of this series (Cayrel et al. 2004), we confirmed the existence of relatively uniform α-element overabundances in 32 very metal-poor halo giants down to [Fe/H] $\simeq -4.2$, as expected for material enriched by massive progenitors. The very small dispersion in [α/Fe] showed that previous findings of significant scatter in [α/Fe] and [Fe-peak/Fe] at low metallicity were due to problems in the data and/or analyses (low S/N, uncertain stellar atmospheric parameters, combinations of data

⋆ Based on observations made with the ESO Very Large Telescope at Paranal Observatory, Chile (program ID 165.N-0276(A); P.I: R. Cayrel).

using different line lists, different analysis techniques, etc.). The results of Paper V thus suggested that mixing of the ISM in the early Galaxy was quite efficient.

In contrast, the neutron-capture elements have been found to behave very differently (Molaro & Bonifacio 1990; Norris et al. 1993; Primas et al. 1994). For example, the [Ba/Fe] and [Sr/Fe] ratios are found to be generally below solar for stars with [Fe/H] < −2.5 (McWilliam et al. 1995; Ryan et al. 1996; McWilliam 1998), but the trends with metallicity differ from one element to another. Moreover, several [n-capture/Fe] ratios exhibit a large spread at low metallicity (McWilliam et al. 1995; Ryan et al. 1996; McWilliam 1998), as confirmed recently by Christlieb et al. (2004) and Barklem et al. (2005) from a large sample of very metal-poor stars.

The detailed abundance ratios between the neutron-capture elements are our best diagnostics of the processes that synthesised these elements in the earliest stars. The detailed characteristics of the dispersion of these ratios around the mean relations (amplitude, change with metallicity, etc.) are also our most important diagnostics of the efficiency of mixing in the early ISM.

As in Paper V, we therefore want to determine, from high-quality spectra analysed in a consistent manner, the precise abundance relations between the main groups of neutron-capture elements seen in the most metal-poor stars and quantify the scatter around these mean relations. For this, we select the same sample of very metal-poor halo giants as discussed earlier in the "First Stars" project, using the same spectra, atmospheric parameters, and analysis techniques as before.

Throughout this paper we will use the designations Very Metal-Poor (VMP), Extremely Metal-Poor (EMP), and Ultra Metal-Poor (UMP) for stars with metallicities −3 < Fe/H] < −2, −4 < Fe/H] < −3, and [Fe/H] < −4, respectively (Beers & Christlieb 2005). We will not discuss the Carbon-Enhanced Metal-Poor (CEMP) stars, many of which exhibit peculiar abundances and may be binary systems (Lucatello et al. 2004, and in preparation).

2. Observations

The observations were performed during several observing runs in 1999 and 2000 at the VLT-Kueyen telescope with the high-resolution spectrograph UVES (Dekker et al. 2000). Details of these observations and the spectrograph settings were given in Paper V, which also provided abundances of the lighter elements for the same sample of stars as studied here.

The spectra were reduced using the UVES package within MIDAS, which performs bias and inter-order background subtraction (object and flat-field), optimal extraction of the object (above sky, rejecting cosmic-ray hits), division by a flat-field frame extracted with the same weighted profile as the object, wavelength calibration, rebinning to a constant wavelength step, and merging of all overlapping orders. The spectra were then added and normalized to unity in the continuum.

Because UVES is so efficient in the near UV, we achieve typical S/N ratios per resolution element of 50 or more at 350 nm. Thus, the weak lines from the heavy elements become measurable even in the EMP stars of our sample; most previous studies were based on spectra of substantially lower quality.

3. Abundance analysis

As described in Paper V, a classical LTE analysis of our spectra was carried out, using OSMARCS model atmospheres (Gustafsson et al. 1975; Plez et al. 1992; Edvardsson et al. 1993; Asplund et al. 1997; Gustafsson et al. 2003). Abundances were determined with a current version of the `turbospectrum` code (Alvarez & Plez 1998), which treats scattering in detail. Solar abundances were adopted from Grevesse & Sauval (2000).

Line detection and equivalent-width measurement was first carried out with the line list of the appendix of Paper I (Hill et al. 2002) and the automatic code `fitline`, which is based on genetic algorithms. As most of the lines are weak and located in crowded spectral regions, this turned out to be less than optimal, so we decided to determine the abundances by fitting synthetic spectra to all visible lines (and therefore do not list individual measured equivalent widths here).

It soon became clear that establishing upper limits for the abundances of many of the heavy elements could also be useful, even when no line from the strongest predicted transition could be detected. These upper limits were computed by comparing the synthetic and observed spectra, and changing the abundance until the computed strength of the line was of the same order as the noise in the observed spectrum.

All the measured abundances and upper limits are given in Tables 3–5 and shown in detail in Figs. 6–9.

3.1. Atmospheric parameters

The procedures employed to derive $T_{\rm eff}$, log g, and micro-turbulent velocity estimates $v_{\rm t}$ for our stars were described in detail in Paper V (Sect. 3). In summary, $T_{\rm eff}$ is derived from broad-band photometry, using the Alonso et al. (1999) calibration. The surface gravity is set by requiring that the Fe and Ti abundances derived from neutral and singly ionised transitions be identical. Micro-turbulent velocities are derived by eliminating the trend in abundance of the Fe I lines as a function of equivalent width. Table 1 lists the atmospheric parameters adopted from Paper V.

3.2. Line list

For all of the stars in our sample, we adopt the [Fe/H] abundances derived in Paper V, which are based on a large number of lines (60–150 Fe I lines and 4–18 Fe II lines). The line list used to determine the heavy-element abundances is taken from Paper I, but updated with recent determinations of oscillator strengths and hyperfine structure corrections (Den Hartog et al. 2003; Lawler et al. 2004) for several of the elements.

The solar abundances from Grevesse & Sauval (2000) have not been corrected for the changes introduced by these corrections, as they are small and only affect some of the transitions in each element.

3.3. Error budget

Table 2 lists the computed errors in the heavy-element abundance ratios due to typical uncertainties in the stellar parameters. These errors were estimated by varying $T_{\rm eff}$, log g, and $v_{\rm t}$ in the model atmosphere of BS 17569-049 by the amounts indicated; other stars of the sample yield similar results. As will be seen, errors in the basic parameters largely cancel out in the abundance ratios between elements in similar stages of ionization and with similar excitation potentials.

The global error of an element abundance [A/H], including errors in fitting of the synthetic line profile to the observed spectra, is of the order of 0.20−0.25 dex, depending on the species

Table 1. The observed sample of stars, with adopted model parameters ($T_{\rm eff}$, log g, $v_{\rm t}$, [Fe/H]$_{\rm m}$) and final iron abundances [Fe/H]$_{\rm c}$ (from Paper V).

Star	$T_{\rm eff}$	log g	$v_{\rm t}$	[Fe/H]$_{\rm m}$	[Fe/H]$_{\rm c}$
HD 2796	4950	1.5	2.1	−2.4	−2.47
HD 186478	4700	1.3	2.0	−2.6	−2.59
BD +17:3248	5250	1.4	1.5	−2.0	−2.07
BD –18:5550	4750	1.4	1.8	−3.0	−3.06
CD –38:245	4800	1.5	2.2	−4.0	−4.19
BS 16467–062	5200	2.5	1.6	−4.0	−3.77
BS 16477–003	4900	1.7	1.8	−3.4	−3.36
BS 17569–049	4700	1.2	1.9	−3.0	−2.88
CS 22169–035	4700	1.2	2.2	−3.0	−3.04
CS 22172–002	4800	1.3	2.2	−4.0	−3.86
CS 22186–025	4900	1.5	2.0	−3.0	−3.00
CS 22189–009	4900	1.7	1.9	−3.5	−3.49
CS 22873–055	4550	0.7	2.2	−3.0	−2.99
CS 22873–166	4550	0.9	2.1	−3.0	−2.97
CS 22878–101	4800	1.3	2.0	−3.0	−3.25
CS 22885–096	5050	2.6	1.8	−4.0	−3.78
CS 22891–209	4700	1.0	2.1	−3.0	−3.29
CS 22892–052	4850	1.6	1.9	−3.0	−3.03
CS 22896–154	5250	2.7	1.2	−2.7	−2.69
CS 22897–008	4900	1.7	2.0	−3.5	−3.41
CS 22948–066	5100	1.8	2.0	−3.0	−3.14
CS 22952–015	4800	1.3	2.1	−3.4	−3.43
CS 22953–003	5100	2.3	1.7	−3.0	−2.84
CS 22956–050	4900	1.7	1.8	−3.3	−3.33
CS 22966–057	5300	2.2	1.4	−2.6	−2.62
CS 22968–014	4850	1.7	1.9	−3.5	−3.56
CS 29491–053	4700	1.3	2.0	−3.0	−3.04
CS 29495–041	4800	1.5	1.8	−2.8	−2.82
CS 29502–042	5100	2.5	1.5	−3.0	−3.19
CS 29516–024	4650	1.2	1.7	−3.0	−3.06
CS 29518–051	5200	2.6	1.4	−2.8	−2.69
CS 30325–094	4950	2.0	1.5	−3.4	−3.30

Table 2. Estimated errors in the element abundance ratios [X/Fe] and [X/Ba] for BS 17569-049. The other stars yield similar results.

[X/Fe]	$\Delta T_{\rm eff}$ = +100 K	Δlog g = +0.2	$\Delta v_{\rm t}$ = +0.2 km s^{-1}
Sr	−0.02	0.03	0.01
Y	−0.01	0.06	0.00
Zr	−0.01	0.07	0.03
Ba	0.02	0.03	−0.02
La	0.00	0.06	0.00
Ce	0.00	0.07	0.05
Pr	0.00	0.07	0.04
Nd	0.00	0.07	0.04
Sm	0.00	0.07	0.05
Eu	0.01	0.01	−0.04
Gd	−0.01	0.07	0.03
Dy	0.00	0.07	0.04
Ho	0.00	0.07	0.02
Er	0.00	0.06	−0.03
Tm	−0.01	0.04	0.02
Yb	0.01	0.06	−0.01
[X/Ba]	$\Delta T_{\rm eff}$ = +100 K	Δlog g = +0.2	$\Delta v_{\rm t}$ = +0.2 km s^{-1}
Sr	−0.04	0.00	0.03
Y	−0.03	0.03	0.02
Zr	−0.03	0.04	0.05
Ba	... .	...	...
La	−0.02	0.03	0.02
Ce	−0.02	0.04	0.07
Pr	−0.02	0.04	0.06
Nd	−0.02	0.04	0.06
Sm	−0.02	0.04	0.07
Eu	−0.01	−0.02	−0.02
Gd	−0.03	0.04	0.05
Dy	−0.02	0.04	0.06
Ho	−0.02	0.04	0.04
Er	−0.02	0.03	−0.01
Tm	−0.01	0.01	0.05
Yb	−0.01	−0.03	0.01

under consideration. The typical line-to-line scatter (standard deviation) for a given element is 0.05−0.15 dex.

4. Abundances of the neutron-capture elements

4.1. The light neutron-capture elements Sr, Y, and Zr

In the Solar System, the abundances of Sr, Y, and Zr are dominated by *s*-process production (Arlandini et al. 1999). A small fraction of these elements can be produced by the weak *s*-process (Prantzos et al. 1990), but this process is not expected to be efficient at the low metallicities observed in our sample.

Figure 1 shows the abundance ratios [Sr/Fe], [Y/Fe], and [Zr/Fe] as functions of [Fe/H], as determined here and by Honda et al. (2004), together with data selected from earlier papers (Ryan et al. 1991; Norris et al. 2001; Gratton et al. 1987; Gilroy et al. 1988; Gratton et al. 1988; Gratton & Sneden 1991; Edvardsson et al. 1993; Gratton & Sneden 1994; McWilliam et al. 1995; Carney et al. 1997; Nissen & Schuster 1997; McWilliam 1998; Stephens 1999; Burris et al. 2000; Fulbright 2000; Carretta et al. 2002; Johnson & Bolte 2002). Only results based on high-resolution, high-S/N spectroscopy are shown here; thus we do not include the recent lower-S/N data by Barklem et al. (2005).

Figure 1 shows a rather similar behaviour for these three elements, i.e. [X/Fe] $\simeq$ 0 for stars with [Fe/H] above $\simeq$–3.0. Below this metallicity, all the abundance ratios drop below the solar values. In other words, the progressive enrichment in these elements only reaches the solar ratio at about [Fe/H] = −3.0.

4.1.1. Strontium

Strontium is a key element for probing the early chemical evolution of the Galaxy, because its resonance lines are strong and can be measured even in stars with metallicities as low as [Fe/H] = −4.0. For most of our stars, only the resonance lines at 4077.719 Å and 4215.519 Å are visible in our spectra.

We adopt the gf values from Sneden et al. (1996) and confirm the large underabundance of Sr in EMP stars reported e.g. by Honda et al. (2004). It has long been realized that the [Sr/Fe] ratio exhibits very high dispersion for stars with [Fe/H] ≤ -2.8 (McWilliam et al. 1995; Ryan et al. 1996), and we confirm this as well. As typical errors in the [Sr/Fe] ratio are no more than a few tenths of a dex at worst, this large spread (over 2 dex) cannot be attributed to observational errors; see, e.g., Ryan et al. (1996).

4.1.2. Yttrium

The Y lines are somewhat weaker than those of Sr in this temperature range and are not readily detected in our most metal-poor stars. However, nine lines of similar strength (354.9 nm, 360.07 nm, 361.10 nm, 377.43 nm, 378.86 nm, 381.83 nm, 383.29 nm, 395.03 nm, and 439.80 nm) can be measured in stars

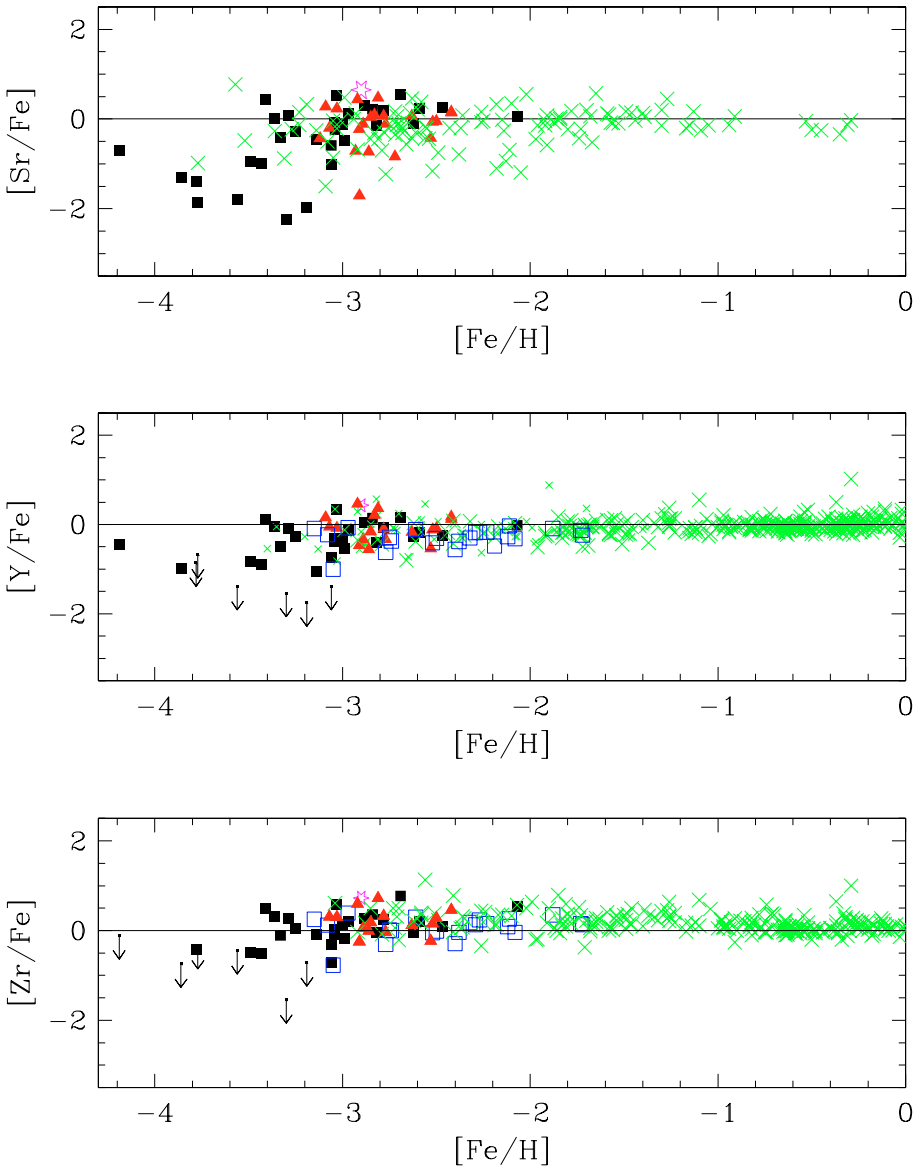

Fig. 1. The abundance ratios [Sr/Fe], [Y/Fe], and [Zr/Fe] as functions of [Fe/H]. *Black rectangles*: present study; *red triangles*; Honda et al. (2004); *blue rectangles*: Johnson & Bolte (2002); *green crosses*: selected results from earlier literature (see references listed in text). CS 31082-001 (Paper I) is shown by a *magenta star*.

with [Fe/H] > −3.5 when the temperature is low enough, and then yield rather robust abundance determinations for Y.

The middle panel of Fig. 1 shows [Y/Fe] as a function of [Fe/H]. The overall trend is similar to that found for Sr, i.e., a solar ratio down to [Fe/H] ≃ −3.0, and lower values of increasing dispersion at even lower metallicities. Unlike Sr, which displays a relatively high dispersion at all metallicities, the weaker and sharper lines of Y yield a very small dispersion in its abundance at intermediate or higher metallicities. The similarity we stress here is that the dispersions in both [Sr/H] and [Y/H] increase by at least a factor of 2 below [Fe/H] ≃ −3.0.

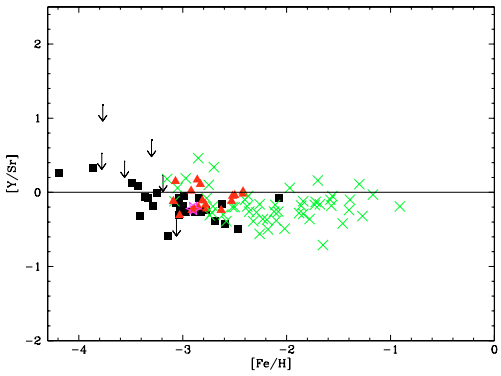

Fig. 2. [Y/Sr] as a function of [Fe/H]. Symbols as in Fig. 1.

4.1.3. Zirconium

Zr is similar to Y in line strength, and we can measure 5–10 lines in stars with [Fe/H] > −3.50 (see Fig. 1). We find a similar pattern for [Zr/Fe] as for Sr and Y, with a slightly lower average underabundance, large dispersion below [Fe/H] ≃ −3.0, and somewhat smaller scatter at intermediate and higher metallicities.

4.1.4. The [Y/Sr] ratio

If two elements are formed by the same process, their ratio should not vary with metallicity, and the dispersion around the mean value should yield a good estimate of the errors on the abundance determinations. Figure 2 shows the ratio [Y/Sr] as a function of [Fe/H] for our data, along with those by

Table 3. Abundance results. Numbers in parenthesis indicate the number of lines measured.

Object	[Fe/H]	[Sr/Fe]	[Y/Fe]	[Zr/Fe]	[Ba/Fe]	[La/Fe]	[Ce/Fe]
HD 2796	−2.47	+0.25 (3)	−0.25 (10)	+0.08 (17)	−0.14 (2)	−0.10 (7)	+0.06 (2)
HD 186478	−2.59	+0.24 (3)	−0.19 (9)	+0.21 (14)	−0.04 (4)	+0.05 (5)	+0.01 (15)
BD +17:3248	−2.07	+0.05 (3)	−0.02 (3)	+0.53 (5)	+0.69 (2)	+0.66 (5)	+0.49 (2)
BD −18:5550	−3.06	−1.01 (2)	<–1.38	−0.71 (5)	−0.74 (4)	<–0.91	<–0.42
CD −38:245	−4.19	−0.71 (3)	−0.45 (2)	<–0.11	−0.76 (2)	<+0.02	<+0.71
BS 16467-062	−3.77	−1.85 (2)	<–0.67	<–0.33	<–1.16	<+0.30	<+1.19
BS 16477-003	−3.36	+0.01 (2)	−0.05 (9)	+0.31 (13)	−0.45 (4)	<–0.01	<+0.38
BS 17569-049	−2.88	+0.31 (2)	+0.04 (10)	+0.27 (17)	+0.20 (4)	+0.38 (7)	+0.23 (9)
CS 22169-035	−3.04	−0.08 (2)	−0.38 (10)	−0.08 (15)	−1.19 (2)	<–0.93	<–0.34
CS 22172-002	−3.86	−1.31 (2)	−0.98 (1)	<–0.74	−1.17 (2)	<–0.01	<+0.58
CS 22186-025	−3.00	−0.12 (2)	−0.31 (9)	+0.14 (15)	+0.02 (4)	+0.19 (6)	+0.27 (1)
CS 22189-009	−3.49	−0.95 (2)	−0.83 (1)	−0.49 (1)	−1.29 (2)	<–0.18	<+0.41
CS 22873-055	−2.99	−0.48 (2)	−0.53 (9)	−0.17 (15)	−0.45 (4)	−0.47 (5)	<–0.09
CS 22873-166	−2.97	+0.13 (2)	−0.13 (9)	+0.20 (15)	−0.70 (4)	−0.77 (3)	−0.34 (2)
CS 22878-101	−3.25	−0.27 (2)	−0.28 (9)	+0.05 (6)	−0.58 (2)	−0.42 (1)	<+0.17
CS 22885-096	−3.78	−1.39 (2)	<–0.86	−0.42 (1)	−1.10 (1)	<–0.09	<+0.90
CS 22891-209	−3.29	+0.08 (2)	−0.10 (9)	+0.26 (12)	−0.55 (4)	−0.28 (1)	<–0.19
CS 22892-052	−3.03	+0.53 (3)	+0.33 (10)	+0.58 (17)	+1.01 (5)	+1.11 (6)	+1.02 (14)
CS 22896-154	−2.69	+0.54 (2)	+0.15 (2)	+0.77 (4)	+0.51 (3)	+0.42 (1)	+0.71 (2)
CS 22897-008	−3.41	+0.44 (2)	+0.12 (4)	+0.50 (4)	−1.00 (2)	<–0.46	<+0.33
CS 22948-066	−3.14	−0.46 (2)	−1.05 (2)	−0.09 (3)	−0.94 (3)	<–0.73	<–0.04
CS 22952-015	−3.43	−0.99 (2)	−0.90 (7)	−0.52 (3)	−1.33 (3)	<–0.54	<+0.05
CS 22953-003	−2.84	+0.22 (3)	+0.14 (10)	+0.36 (11)	+0.49 (5)	+0.66 (7)	+0.66 (2)
CS 22956-050	−3.33	−0.42 (2)	−0.49 (5)	−0.11 (2)	−0.78 (3)	<–0.24	<+0.25
CS 22966-057	−2.62	−0.10 (2)	−0.26 (6)	−0.04 (3)	−0.24 (4)	+0.25 (1)	<+0.34
CS 22968-014	−3.56	−1.80 (2)	<–1.38	<–0.44	−1.77 (1)	−0.11 (1)	<+0.48
CS 29491-053	−3.04	−0.24 (2)	−0.31 (10)	+0.02 (9)	−0.89 (4)	<–0.93	<–0.34
CS 29495-041	−2.82	−0.15 (2)	−0.41 (10)	−0.04 (16)	−0.65 (4)	−0.45 (1)	<–0.16
CS 29502-042	−3.19	−1.98 (2)	<–1.75	<–0.71	−1.69 (2)	<–0.58	<+0.51
CS 29516-024	−3.06	−0.59 (2)	−0.74 (7)	−0.31 (3)	−0.90 (2)	−0.61 (1)	<–0.32
CS 29518-051	−2.78	+0.18 (2)	−0.06 (10)	+0.25 (11)	−0.45 (2)	−0.49 (1)	<+0.20
CS 30325-094	−3.30	−2.24 (2)	<–1.54	<–1.54	−1.88 (2)	<–0.27	+0.42 (1)

Burris et al. (2000), Johnson & Bolte (2002), and Honda et al. (2004). We confirm that [Y/Sr] is constant with rather low scatter around the mean value: $[\langle Y/Sr\rangle] = -0.2 \pm 0.2$ (s.d.). This dispersion is fully accounted for by the observational errors, indicating that any cosmic scatter in this ratio is very small.

However, a plot of [Y/Sr] as a function of [Sr/H] from our data and those by Johnson & Bolte (2002) (Fig. 5), appears to show an anticorrelation between [Y/Sr] and [Sr/H] – a result that needs confirmation as some of the data points are upper limits only. This is not seen in the data set of Honda et al. (2004), as the range of Sr abundances in their sample is fairly small.

4.1.5. General features of the first neutron-capture peak elements

The first-peak elements are known to have a more complex origin than the heavier neutron-capture elements like Ba or Eu, which are only produced by the "main" components of the *r*- and *s*-processes. In solar-type material, Sr, Y and Zr are formed in the "main" *s*-process, but at lower metallicity the "weak" *s*-process (Busso et al. 1999) also contributes. In our EMP stars, we expect a pure *r*-process origin for the neutron-capture elements, and we wish to explore the nature of those processes in more detail.

Figure 3 shows the average [⟨Sr + Y + Zr⟩/Fe] ratio for our stars and from recent literature as a function of [Fe/H]. Only stars with data for all three elements are included, which limits the sample towards the lowest metallicities). We find a clear increase in the dispersion of this ratio with decreasing metallicity. Note also that the two most metal-poor stars ([Fe/H] ≃ −3.5) in Fig. 3

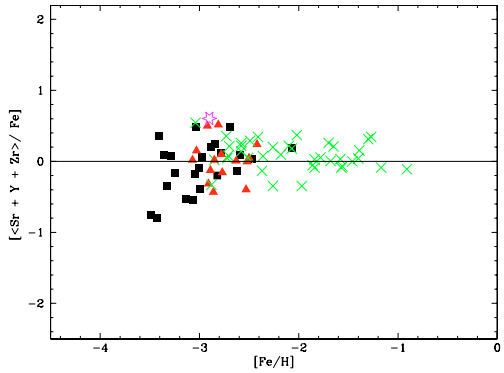

Fig. 3. [⟨Sr, Y, Zr⟩/Fe] vs. [Fe/H]. Symbols as Fig. 1.

are nearly one dex below the solar value, reflecting the strong deficiency of all three elements in the most metal-poor stars.

Because Fe and the neutron-capture elements form under quite different conditions, it may be more informative to study their abundances as functions of another heavy element. The strong resonance lines of Ba can be measured in stars down to almost [Fe/H] = −4.0, so we select Ba as our alternative reference element. Figure 4 shows the mean [⟨Sr + Y + Zr⟩/Ba] ratio as a function of [Ba/H]. We find a striking, tight anti-correlation, especially for stars below [Ba/H] ≃ −2.5), which may indicate that another nucleosynthesis process produces the light neutron-capture elements preferentially at low metallicity. We discuss this point more fully in Sect. 5.2.

Table 4. Abundance results (continued).

Object	[Fe/H]	[Pr/Fe]	[Nd/Fe]	[Sm/Fe]	[Eu/Fe]	[Gd/Fe]	[Dy/Fe]
HD 2796	−2.47	+0.26 (1)	−0.13 (5)	+0.06 (1)	+0.11 (1)	−0.05 (3)	+0.01 (5)
HD 186478	−2.59	+0.25 (2)	+0.32 (8)	+0.41 (2)	+0.48 (2)	+0.41 (2)	+0.33 (16)
BD +17:3248	−2.07	+0.66 (1)	+0.69 (2)	+0.74 (2)	+0.93 (3)	+0.90 (1)	+1.01 (2)
BD −18:5550	−3.06	...	−0.46 (2)	<+0.05	−0.20 (1)	−0.26 (1)	<−0.08
CD −38:245	−4.19	<+0.83	<+0.19	<+1.28	<+0.38	<+0.77	<+0.95
BS 16467-062	−3.77	<+1.31	<+0.57	<+1.46	<+0.76	<+0.75	<+1.43
BS 16477-003	−3.36	<+0.40	<+0.36	<+0.65	<+0.25	<+0.44	<+0.72
BS 17569-049	−2.88	+0.75 (3)	+0.43 (17)	+0.89 (2)	+0.72 (1)	+0.62 (3)	+0.59 (9)
CS 22169-035	−3.04	<+0.18	<−0.76	<−0.07	<−0.67	<−0.28	<−1.10
CS 22172-002	−3.86	<+0.50	<−0.04	<+1.05	<+0.05	+0.54 (2)	<−0.08
CS 22186-025	−3.00	+0.24 (1)	+0.28 (3)	<+0.59	+0.54 (1)	+0.68 (1)	+0.53 (2)
CS 22189-009	−3.49	<+0.23	<−0.11	<+0.88	<−0.02	+1.12 (2)	<−0.35
CS 22873-055	−2.99	−0.27 (1)	−0.29 (2)	<+0.18	−0.17 (1)	−0.03 (2)	−0.24 (3)
CS 22873-166	−2.97	−0.04 (1)	−0.25 (3)	<−0.04	−0.30 (1)	<−0.55	<−0.87
CS 22878-101	−3.25	<+0.09	<−0.45	<+0.34	−0.06 (1)	<−0.07	−0.29 (1)
CS 22885-096	−3.78	<+0.62	<+0.58	<+1.27	<+0.47	<+0.86	<+0.24
CS 22891-209	−3.29	+0.13 (1)	−0.36 (1)	<+0.28	−0.09 (1)	−0.13 (1)	−0.62 (1)
CS 22892-052	−3.03	+0.92 (1)	+1.15 (22)	+1.50 (4)	+1.49 (1)	+1.45 (8)	+1.54 (18)
CS 22896-154	−2.69	+0.73 (1)	+0.67 (2)	+0.78 (1)	+0.86 (1)	+0.87 (1)	+0.97 (2)
CS 22897-008	−3.41	<+0.50	+0.01 (1)	<+0.50	<−0.20	<+0.29	<−0.63
CS 22948-066	−3.14	<−0.02	<−0.56	<−0.26	<−0.57	<−0.08	<−0.80
CS 22952-015	−3.43	<+0.07	<−0.37	<−0.37	<−0.28	<+0.01	<−0.71
CS 22953-003	−2.84	+0.68 (1)	+0.72 (2)	+0.34 (2)	+1.05 (1)	+1.01 (4)	+1.04 (12)
CS 22956-050	−3.33	<+0.37	<−0.17	<+0.03	<+0.02	<+0.21	<−0.31
CS 22966-057	−2.62	<+0.76	+0.47 (2)	<+0.32	+0.41 (1)	<+0.30	+0.48 (1)
CS 22968-014	−3.56	<+0.40	<−0.14	<+0.16	<+0.05	<+0.14	<−0.28
CS 29491-053	−3.04	<−0.12	−0.46 (1)	<−0.46	−0.42 (1)	<−0.38	<−0.80
CS 29495-041	−2.82	−0.14 (1)	+0.28 (2)	<−0.38	−0.09 (1)	−0.25 (2)	<−0.62
CS 29502-042	−3.19	<+0.23	<−0.31	<−0.21	<−0.22	<+0.07	<+0.55
CS 29516-024	−3.06	<+0.10	−0.44 (1)	<−0.54	−0.25 (1)	<−0.36	−0.59 (1)
CS 29518-051	−2.78	+0.42 (1)	+0.01 (2)	<−0.12	<−0.13	<−0.04	<+0.26
CS 30325-094	−3.30	<+0.64 (1)	0.00 (1)	<0.49	<−0.11	<+0.18	<−0.34

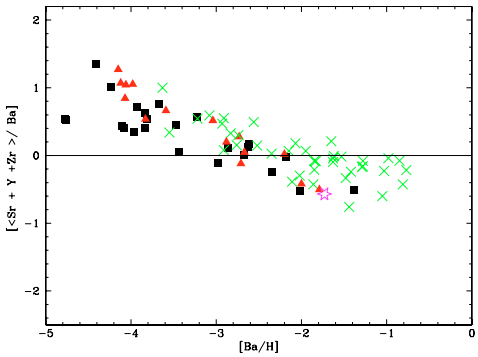

Fig. 4. [⟨Sr, Y, Zr⟩/Ba] vs. [Ba/H]. Symbols as Fig. 1.

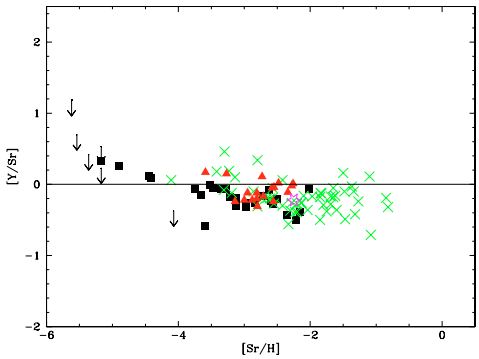

Fig. 5. [Y/Sr] vs. [Sr/H]. Symbols as in Fig. 1.

4.2. The second neutron-capture peak elements (56 ≤ Z ≤ 72)

This range in atomic mass includes the well-studied elements Ba, Eu, and La. Ba and Eu played a key role in understanding early nucleosynthesis, when Truran (1981) first suggested that the [Ba/Eu] vs. [Fe/H] observations of Spite & Spite (1978) could be naturally understood if both of these neutron-capture elements were synthesised by the *r*-process in massive stars during early Galactic evolution (85% of the Ba in the Solar System is due to the *s*-process).

Due to the high UV efficiency of UVES, we have been able to determine abundances or upper limits in many of our stars for several other heavy neutron-capture elements (Ce, Pr, Nd, Sm, Gd, Dy, Ho, Er and Tm). The results are shown in Figs. 10–13 as functions of [Fe/H], together with those by Johnson & Bolte (2002), Honda et al. (2004), and data selected from earlier literature. These data enable us to discuss the nature of the early *r*-process nucleosynthesis in considerable detail.

As noted above, Ba is a particularly interesting element, in part because the resonance lines are strong enough to be measured in all but two of our stars and permit us to explore mean trends and scatter amongst the neutron-capture elements down to [Fe/H] = −4.2; see Fig. 10. All our abundance results for Ba have been derived assuming the isotopic composition corresponding to the *r*-process (McWilliam 1998).

In the metallicity range −2.5 to −3.0, we confirm the very large dispersion in [Ba/Fe] at given [Fe/H] noted by several previous authors, increasing towards the lowest metallicities. Our study adds a significant number of stars below [Fe/H] = −3.0.

Table 5. Abundance results (continued).

Object	[Fe/H]	[Ho/Fe]	[Er/Fe]	[Tm/Fe]	[Yb/Fe]
HD 2796	−2.47	+0.01 (1)	+0.11 (2)	<+1.26	−0.13 (1)
HD 186478	−2.59	<+0.43 (1)	+0.47 (3)	+0.75 (1)	+0.52 (1)
BD +17:3248	−2.07	+0.91 (1)	+1.24 (2)	...	...
BD –18:5550	−3.06	−0.20 (1)	−0.12 (2)	...	...
CD –38:245	−4.19	<+0.53	<+0.86	...	...
BS 16467-062	−3.77	<+1.71	<+1.14	...	...
BS 16477-003	−3.36	<+0.80	<+0.53	...	...
BS 17569-049	−2.88	+0.72 (1)	+0.55 (4)	+0.23 (1)	+0.60 (1)
CS 22169-035	−3.04	<–0.42	<–0.29	+1.20 (1)	...
CS 22172-002	−3.86	<+0.70	<+0.53	...	...
CS 22186-025	−3.00	+0.44 (1)	+0.55 (2)	+1.64 (1)	+0.12 (1)
CS 22189-009	−3.49	<+0.83	<+0.56	...	...
CS 22873-055	−2.99	<–0.37	−0.24 (2)	...	...
CS 22873-166	−2.97	<–0.69	−0.36 (1)	...	...
CS 22878-101	−3.25	<+0.19	<+0.02	...	...
CS 22885-096	−3.78	<+0.82	<+0.55	...	...
CS 22891-209	−3.29	<–0.17	−0.24 (1)	...	... −0.60 (1)
CS 22892-052	−3.03	+1.59 (1)	+1.49 (4)	+1.59 (5)	...
CS 22896-154	−2.69	+0.88 (1)	+1.01 (2)	...	...
CS 22897-008	−3.41	<+0.45	<+0.18	...	...
CS 22948-066	−3.14	<–0.02	<–0.09	...	...
CS 22952-015	−3.43	<–0.13	<+0.00	...	...
CS 22953-003	−2.84	+1.18 (1)	+1.06 (2)	...	... +1.02 (1)
CS 22956-050	−3.33	<+0.87	<+0.20	...	...
CS 22966-057	−2.62	<+0.46	+0.64 (2)	...	...
CS 22968-014	−3.56	<+0.10	<+0.43	...	...
CS 29491-053	−3.04	<–0.32	<–0.39	...	...
CS 29495-041	−2.82	<–0.44	+0.04 (1)	...	...
CS 29502-042	−3.19	...	<+0.46	+1.83 (1)	...
CS 29516-024	−3.06	<–0.40	−0.37	...	...
CS 29518-051	−2.78	<–0.48	<–0.35	+2.00 (1)	...
CS 30325-094	−3.30	<+0.34	<+0.07	...	...

Although the number of stars in this range remains small, Fig. 10 suggests that [Ba/Fe] continues to decline to a mean value of [Ba/Fe] = −2.0−−1.0, with a declining scatter as well. This might indicate that the nucleosynthesis processes involved undergo significant changes below [Fe/H] = −3.2.

The greatest scatter in [Ba/Fe] (a factor of 1000) occurs in the metallicity range $-3.2 \leq$ [Fe/H] ≤ -2.8. Thus, if the Ba and Fe in these stars was created by the same class of progenitor objects, their yields would have to vary by a similarly large factor, whatever model of chemical evolution for the early Galaxy one adopts. The yield of Ba could be extremely metallicity-dependent or, perhaps more likely, the early production of Ba and Fe was not correlated with each other, and Ba and Fe were produced in different astrophysical sites, as suggested by Wanajo et al. (2001, and references therein).

As Fig. 10 shows, we do not observe a single star with a [Ba/Fe] ratio above solar below [Fe/H] $\simeq -3.2$; however, we do note that Barklem et al. (2005) do detect at least a few stars with [Ba/Fe] above solar at metallicities down to [Fe/H] $\simeq -3.4$.

The metallicity interval showing the largest scatter in [Ba/Fe] ($-3.2 \leq$ [Fe/H] ≤ -2.8) is also where the extremely *r*-process-enhanced metal-poor stars are found; i.e. those with [r-element/Fe] > +1.0, referred to as r-II stars by Beers & Christlieb (2005). CS 22892-052, CS 31082-001, the eight new r-II stars found by Barklem et al. (2005), and the most recent discovery HE 1523-0909 (Frebel et al. 2007), all fall in this range. It is interesting that both CS 22892-052 and CS 31082-001 fit into the same region of Fig. 10 as the "normal" (non-r-II) stars (albeit at the very upper limit), so these extreme r-II stars are not exceptional as far as the [Ba/Fe] ratio is concerned.

Like Ba, both La and Ce are primarily due to the *s*-process at solar metallicity. For La and Ce, we can determine abundances for stars with [Fe/H] > −3.0, but only upper limits for the more metal-poor stars. It is interesting, however, that we find the same increase of the scatter with declining metallicity in the range $-3.2 <$ [Fe/H] < -2.0 for La and Ce as for Ba. As this is also seen in the data from Honda et al. (2004) and earlier literature (see Fig. 10), there is little doubt as to its reality.

Figure 11 shows our results for [Pr/Fe], [Nd/Fe], and [Sm/Fe], which in Solar-system material are formed by the *s*- and *r*-process in roughly equal proportions. For Pr, the only earlier data are from Honda et al. (2004). We confirm the high [Pr/Fe] ratios found by these authors down to [Fe/H] $\simeq -3.0$. Our upper limits show that a rather large scatter in [Pr/Fe] exists down to [Fe/H] $\simeq -3.0$; for Nd and Sm, the scatter clearly increases with declining metallicity until its maximum at [Fe/H] $\simeq -3.0$. Note that we have Nd measurements for three stars with [Fe/H] < -3.2.

Eu, Gd, and Dy are elements that are produced primarily by the *r*-process, also in Solar-system material (93%, 84%, and 87%, respectively, according to Arlandini et al. 1999). Figure 12 shows that they behave similarly to the other elements of the second neutron-capture peak and display increasing overabundances with declining metallicity, accompanied by increasing scatter. Once again, it appears that the scatter is at maximum at [Fe/H] $\simeq -3.0$, as found by Honda et al. (2004).

Note that for [Eu/Fe], low values ($\leq$0.0) are found only below [Fe/H] $\simeq -3.0$. Barklem et al. (2005) did find stars with high [Eu/Fe] (>0.5) at metallicities lower than [Fe/H] = −3.0, but from a much larger sample of stars than ours. This indicates that

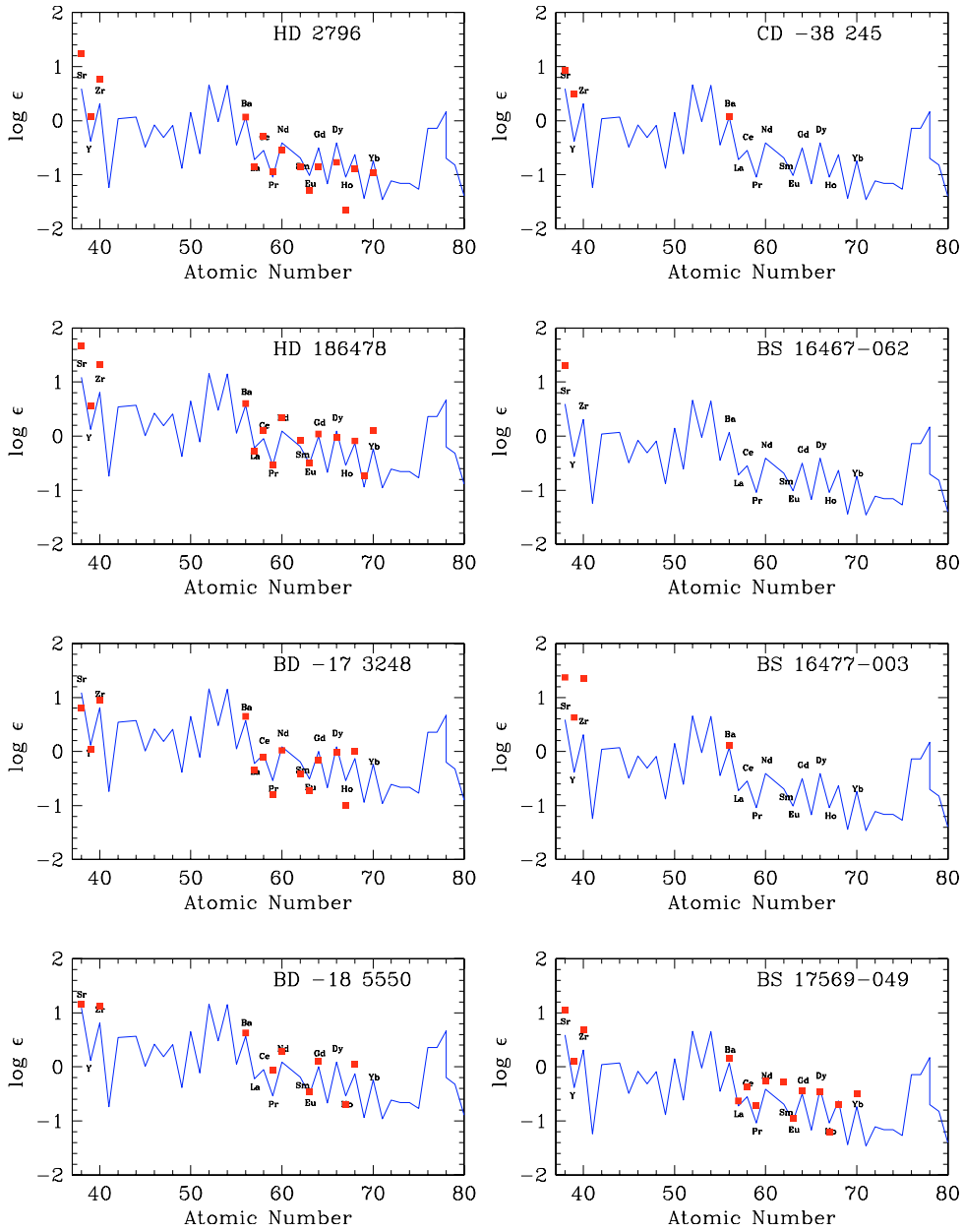

Fig. 6. Abundance patterns for the neutron-capture elements in our sample. The full line shows the Solar-system *r*-process abundance pattern from Arlandini et al. (1999), scaled to match the observed abundance of Ba in each star.

stars with high [Eu/Fe] ratios are quite rare at very low metallicity, so that dedicated surveys are needed to uncover additional examples. For Gd, we do measure high [Gd/Fe] values in two stars (CS 22172-002 and CS 22189-009) below [Fe/H] = −3.4.

Finally, Fig. 13 shows our results for Ho, Er, and Tm, also produced almost exclusively in the *r*-process. Very few previous results exist for these three elements, which we find to be generally overabundant, as also reported by Honda et al. (2004) for Er and Tm. Once more, the large scatter in the element ratios appears maximal at [Fe/H] = −3.0. Our few results for Yb (not plotted) follow the same general trend.

5. Discussion

Our accurate, detailed, and homogeneous abundance data for the neutron-capture elements in a large sample of VMP and EMP stars enables us to address two important questions regarding the first stages of heavy-element enrichment in the Galaxy: *(i)*: the nucleosynthesis process(es) that formed the first heavy elements, and *(ii)*: the efficiency with which the newly synthesised elements were incorporated in the next generation(s) of stars, including those that have survived until today. We discuss each of these in turn in the following.

5.1. Diagnostics of the r-process(es) in EMP stars

We begin by repeating the classical Truran (1981) test of the relative weight of the *r*- and *s*-process as a function of metallicity. Ba and La are produced mostly by the "main" *s*-process in Solar-metallicity stars (92% and 83%, respectively, according to Arlandini et al. (1999), but in EMP stars they should be due to the *r*-process. Figure 14 shows the [Eu/Ba] and [Eu/La] ratios as a function of [Fe/H] for our stars, along with earlier data. The

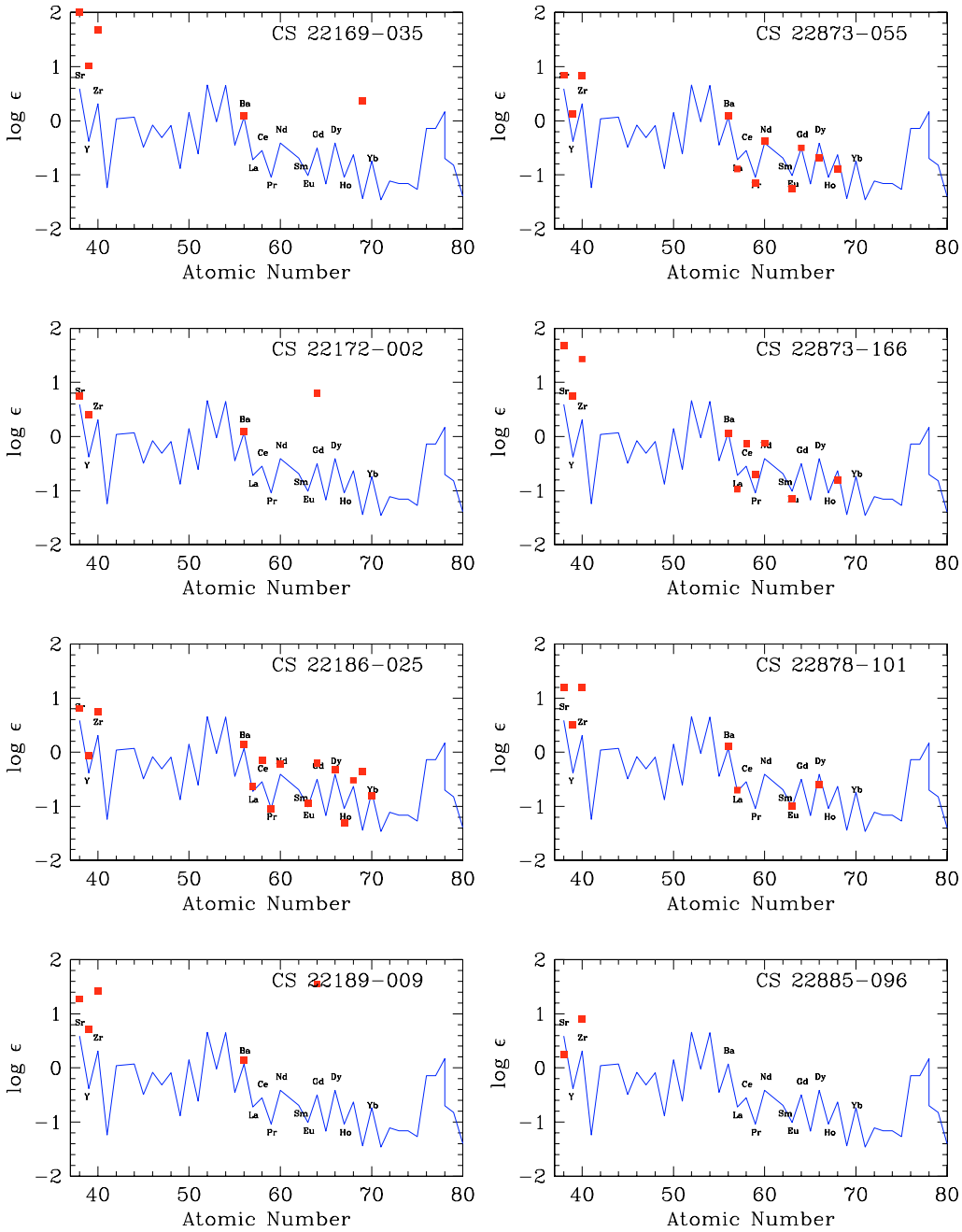

Fig. 7. As Fig. 6, for the next 8 stars.

dashed lines in both panels indicate the Solar-system *r*-process abundance ratios (Arlandini et al. 1999).

Our [Eu/Ba] ratios do cluster around the Solar-system *r*-process value at low metallicity, but a substantial scatter remains. Some of this may be due to the Ba data because of the broad hyperfine structure of the Ba lines: if the mix of Ba isotopes in the star is different from that assumed in the synthetic spectrum, the fit to the observed spectrum may be less stable than for single-component lines. Indeed, the [Eu/La] ratios exhibit substantially smaller dispersion at all metallicities, demonstrating that the scatter in [Eu/Ba] is essentially due to the Ba, not the Eu abundances. Together, the two panels of Fig. 14 confirm that the neutron-capture elements in EMP stars were produced predominantly or exclusively by the *r*-process.

Given the large scatter of the [n-capture element/Fe] ratios as functions of [Fe/H] (Figs. 1 and 10–13), we proceed to compare elemental abundances within the neutron-capture group itself in the following. As noted earlier, we choose Ba as the reference element because data are available for nearly all our stars.

Figure 15 shows the [Sr/Ba], [Y/Ba], and [Zr/Ba] ratios vs. [Ba/H] as determined by us and previous authors. We find a tight anti-correlation of [X/Ba] with [Ba/H] for all three elements, at least down to [Ba/H] = −4.5. We emphasize that most stars in our sample are *not* enriched in *r*-process elements, but note that the two extreme r-II stars CS 22892-052 and CS 31082-001 do in fact follow the same relation as the "normal" stars. In particular, we find no stars that are both Sr-poor and Ba-rich, as suspected already by Honda et al. (2004); however, such cases *are* found among the C-enhanced metal-poor (CEMP) stars (Sivarani et al. 2006).

Our most Ba-poor stars, below [Ba/H] ≃ −4.5, seem to depart from the correlation and show roughly Solar values for

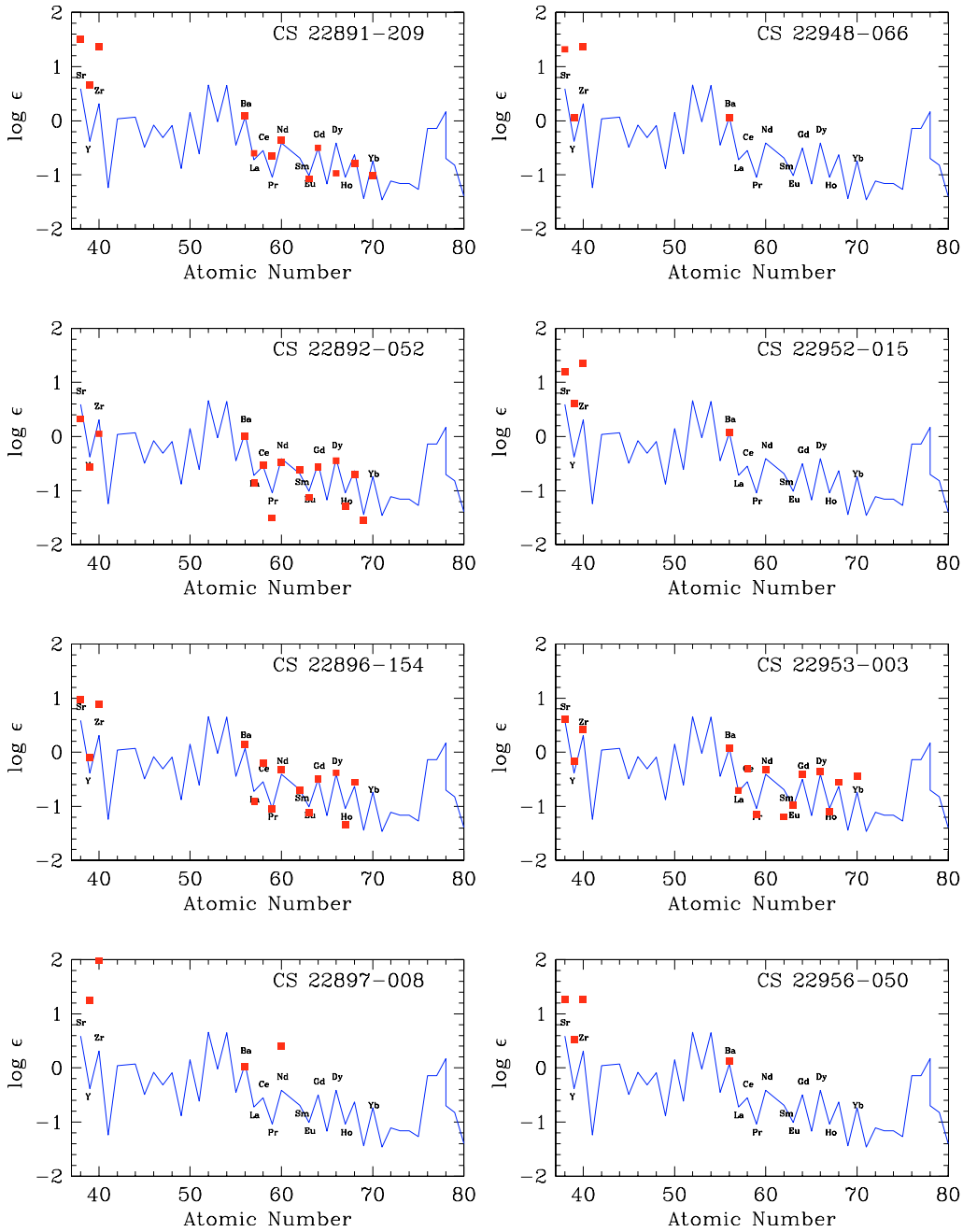

Fig. 8. As Fig. 6, for the next 8 stars.

[Sr/Ba] and [Y/Ba], although we note that Honda et al. (2004) do find a couple of high [Sr/Ba] ratios in this region. This might indicate that the additional production channel for Sr, Y, and Ba discussed below may not operate in the very first stellar generations. However, the sample is very small (these are among our most metal-poor stars, with [Fe/H] < -3.2), and more reliable measurements of Sr, Y, and Zr in stars with low [Ba/H] will be needed for a definitive conclusion.

5.2. Synthesis of the first-peak elements

The diagrams discussed above amply demonstrate that not all the neutron-capture elements in metal-poor stars were produced by a single *r*-process, as discussed by Travaglio et al. (2004, and references therein); an additional process must contribute preferentially to the production of the first-peak elements in VMP/EMP stars, previously called the "weak" *r*-process; we will discuss below the aptness of this term.

Travaglio et al. (2004) explored the issue by following the Galactic enrichment of Sr, Y, and Zr using homogeneous chemical evolution models. They confirmed that a process of primary nature (*r*-process) is required to explain the observed abundance trends, argued that massive stars were the likely sites as these elements occur at very low metallicity, and coined the term "Lighter-Element Primary Process" (LEPP) for it. However, regardless of nomenclature, the actual process, site, or progenitor stars have not been identified.

Cescutti et al. (2005) came to similar conclusions, based on the behavior of Ba and Eu. They confirmed the need for a primary source to explain the behaviour of [Ba/Fe] vs. [Fe/H] and suggested that the primary production of Eu and Ba is associated with stars in the mass range 10–30 $M_{\odot}$. Ishimaru et al. (2004)

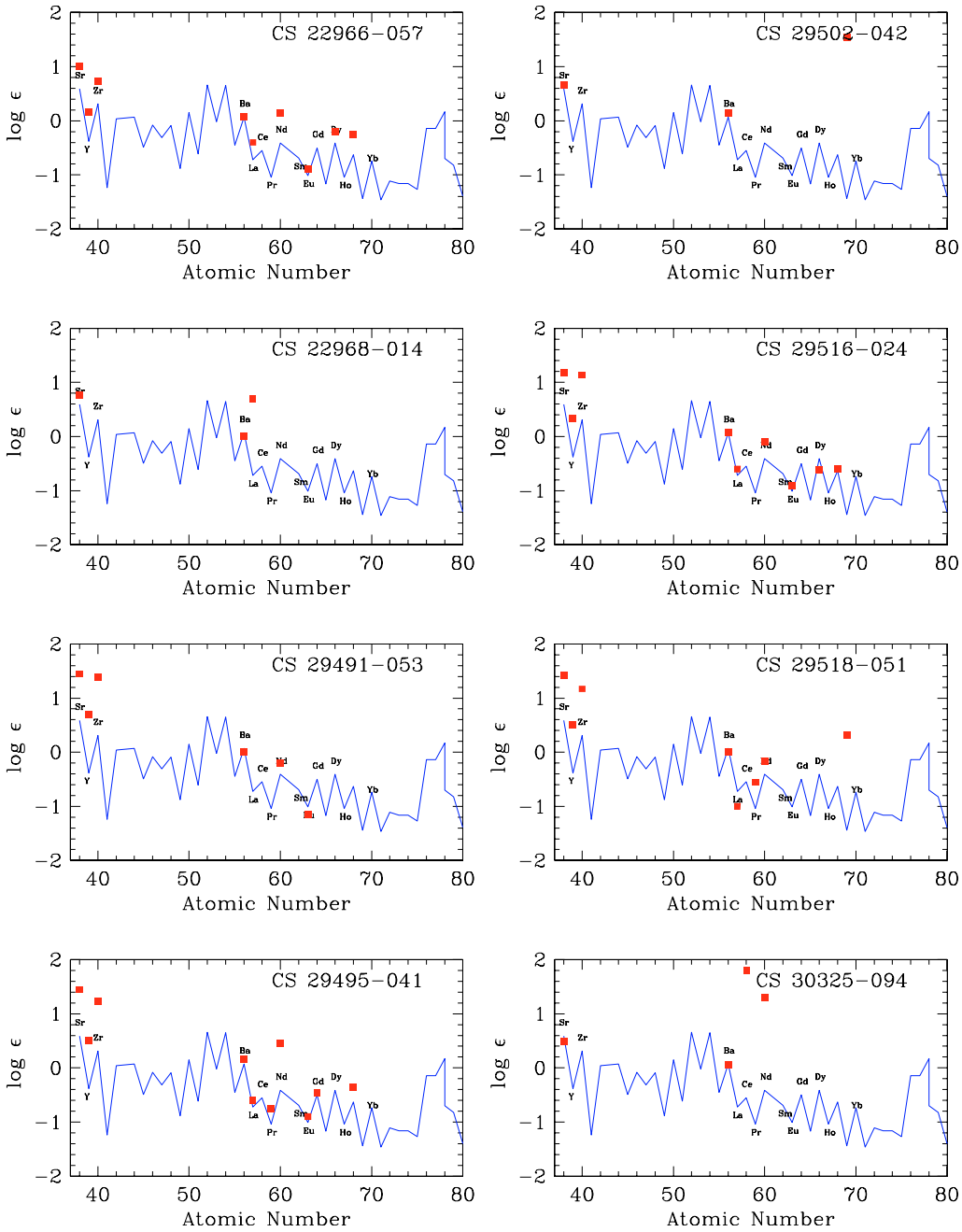

Fig. 9. As Fig. 6, for the last 8 stars.

computed the evolution of [Eu/Fe], using inhomogeneous chemical evolution models with induced star formation, and concluded that the observations implied that the low-mass range of supernovae were the dominant source of Eu.

The observations shown in Fig. 15 clearly cannot be explained by single *r*-process. The trends suggest the existence of three different regimes: *(i)*: [Ba/H] ≥ -2.5, where all ratios are close to Solar; *(ii)*: $-4.5 \leq$ [Ba/H] ≤ -2.5, where Sr, Y, and Zr become increasingly overabundant relative to Ba at lower metallicities, and *(iii)*: [Ba/H] ≤ -4.5, where the abundance ratios seem to drop to Solar again. The latter transition corresponds to [Fe/H] $\simeq -3$, i.e. the metallicity range in which *all* the highly *r*-process enriched metal-poor stars are have been found so far – the r-II stars as defined by Beers & Christlieb (2005).

It appears from these plots, and from the great uniformity of the *r*-process element patterns in the r-II stars observed so far, that the main *r*-process dominates the total abundance pattern of the heavy elements once they have been enriched beyond the level of [Ba/H] ≥ -2.5. At levels up to 2 dex below this threshold, another process contributes increasingly to the production of the first-peak elements Sr, Y, and Zr. We want to clarify the properties of this process as independently of the main *r*-process as possible.

To do so, we have computed the mean residuals of Sr, Y, and Zr in each of our stars from the Solar-system *r*-process abundance pattern of Arlandini et al. (1999) as shown in Figs. 6–9. Thus, these abundance residuals should represent the pure production of the unknown process, free of interference from the main *r*-process.

The result is shown in Fig. 16 and shows that, far from being "weak", the LEPP is responsible for 90–95% of the total abundance of these elements at [Ba/H] $\simeq -4.3$, where

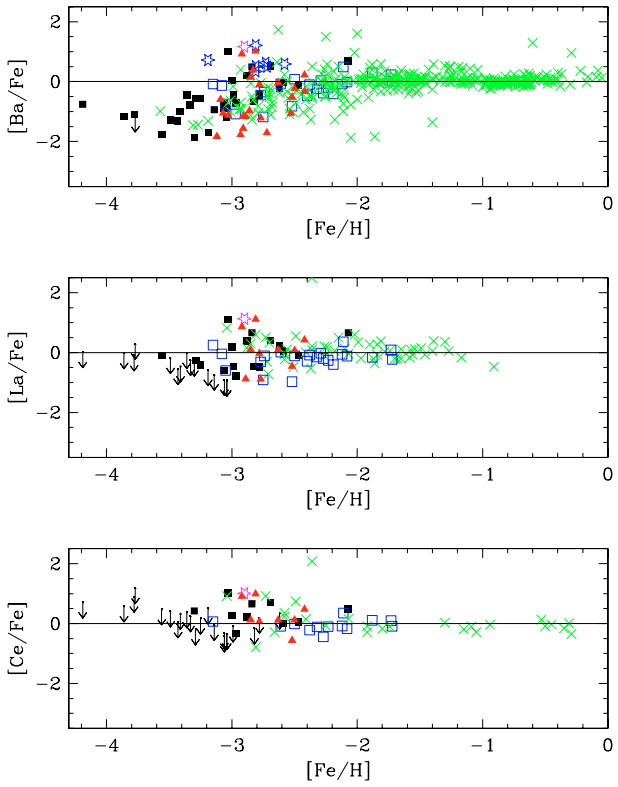

Fig. 10. [Ba/Fe], [La/Fe], and [Ce/Fe] as functions of [Fe/H]. Symbols as in Fig. 1. Blue stars in the upper panel: data from Barklem et al. (2005).

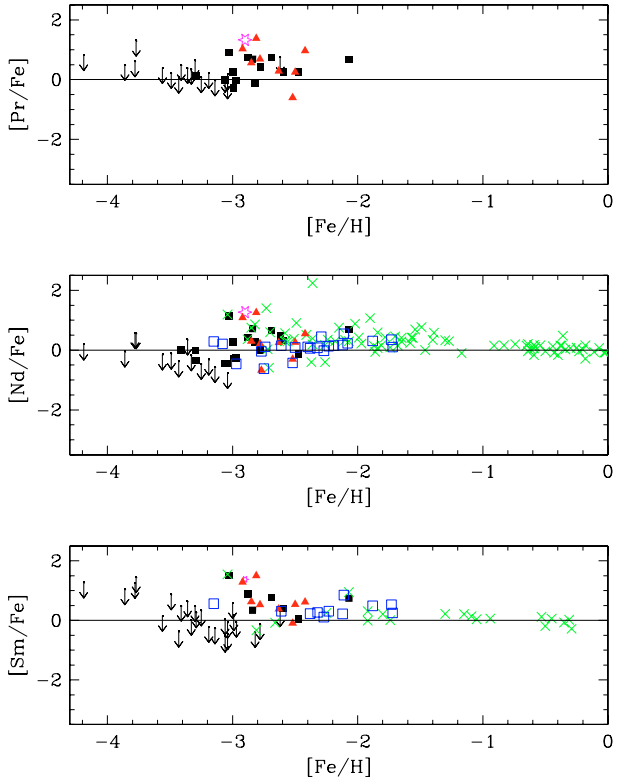

Fig. 11. [Pr/Fe], [Nd/Fe], and [Sm/Fe] as functions of [Fe/H]. Symbols as in Fig. 1.

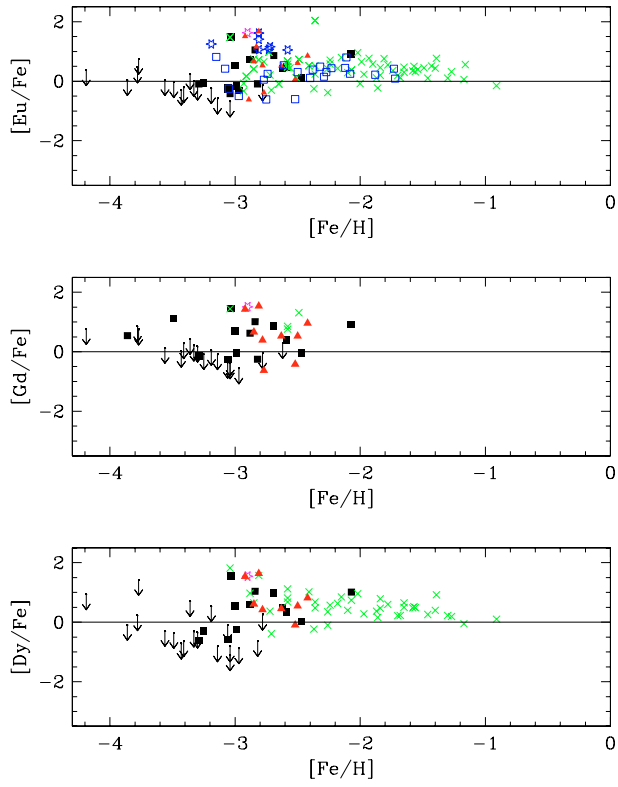

Fig. 12. [Eu/Fe], [Gd/Fe], and [Dy/Fe] as functions of [Fe/H]. Symbols as in Fig. 1. Blue stars in the upper panel: Data from Barklem et al. (2005).

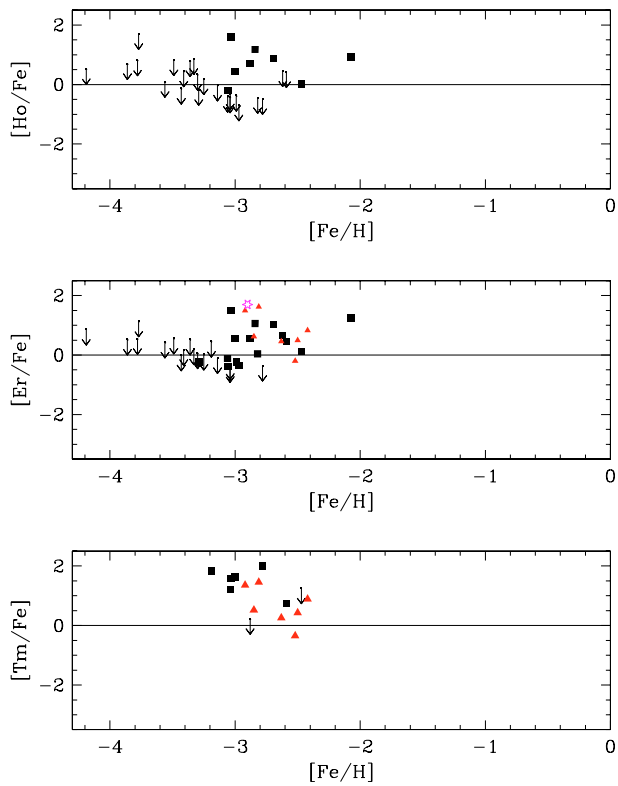

Fig. 13. [Ho/Fe], [Er/Fe], and [Tm/Fe] as functions of [Fe/H]. Symbols as in Fig. 1.

the [⟨Sr, Y, Zr⟩/Ba] ratio may split into two branches, as suggested on theoretical grounds by Ishimaru & Wanajo (1999) and Ishimaru & Wanajo (2000).

One would surmise that qualitative differences in neutron exposure or the nature of the available seed nuclei in the most extreme metal-poor stars could cause such differences. E.g.,

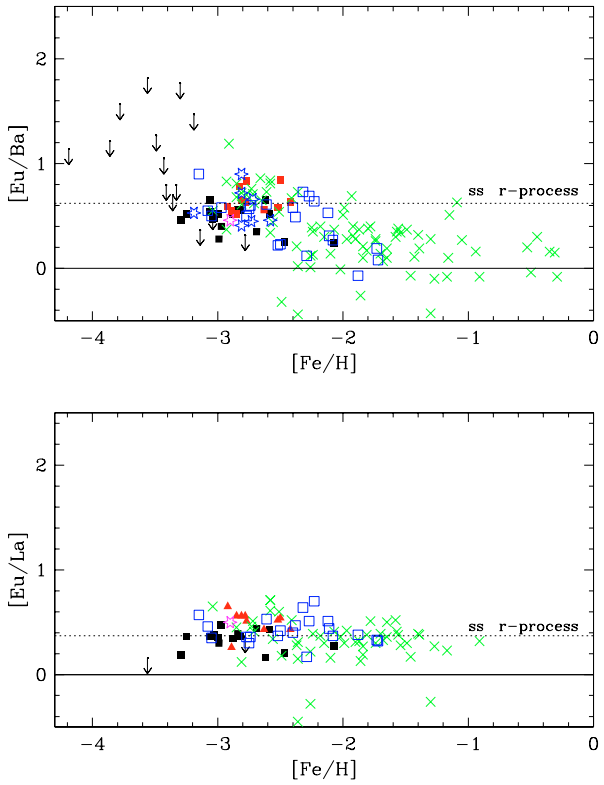

Fig. 14. [Eu/Ba] and [Eu/La] as function of [Fe/H]; symbols as in previous figures. The dashed lines indicate the Solar-system *r*-process abundance ratios (Arlandini et al. 1999).

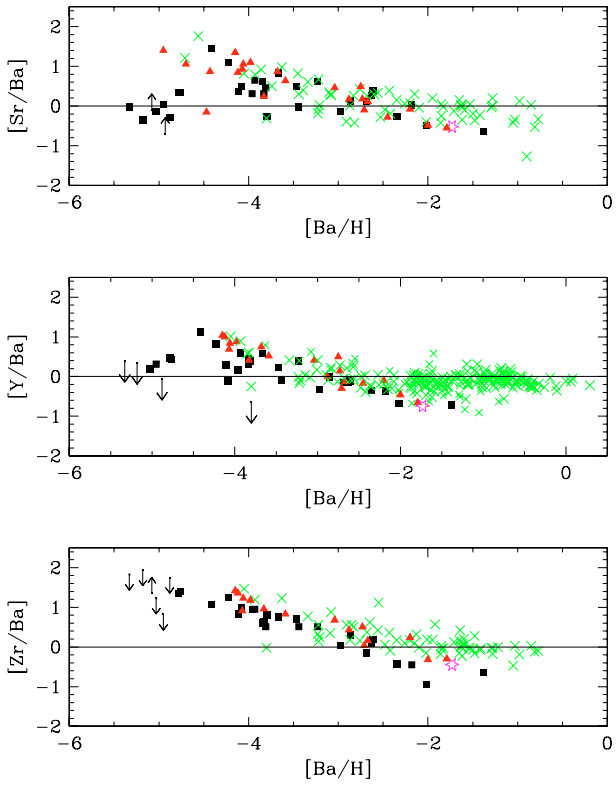

Fig. 15. [Sr/Ba], [Y/Ba], and [Zr/Ba] vs. [Ba/H]. Symbols as in Fig. 1.

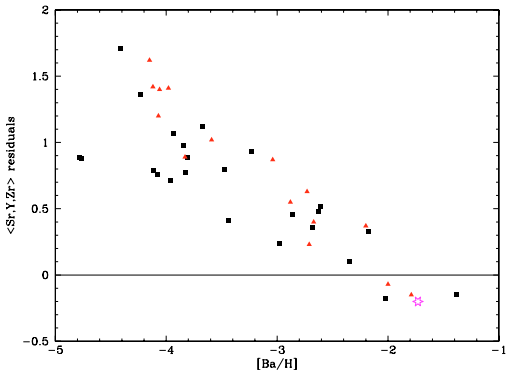

Fig. 16. Average abundance residuals of Sr, Y, and Zr from the Solar-system curves in Figs. 6–9 vs. overall heavy-element content as measured by [Ba/H]. Symbols as Fig. 1.

Qian & Wasserburg (2007) propose that the first-peak elements (Sr, Y, Zr) are formed by charged-particle reactions in the so-called α-process (Woosley & Hoffmann 1992) in all supernovae, while heavy *r*-process elements would form only in low-mass SNe with O-Ne-Mg cores and iron only in high-mass SNe. The correlation shown in Fig. 16 would appear difficult to reconcile with this otherwise interesting scenario.

As an alternative, a new nucleosynthesis process (the *νp*-process) has been proposed very recently by Froehlich et al. (2006). This process should occur in core-collapse supernovae and would allow for the nucleosynthesis of nuclei with mass number $A > 64$.

5.3. Heavy-element enrichment in the early Galaxy

The scatter in the observed abundance ratios are an indication of the efficiency of mixing in the ISM in the era before the formation of the oldest stars we can observe today. The results so far are contradictory.

In Paper V, we demonstrated that the [α/Fe] ratios in the EMP giant stars of our sample exhibit very little scatter beyond the observational uncertainty. The great uniformity in the [α/Fe] ratios of metal-poor stars has recently been demonstrated in more limited samples of turnoff (dwarf) stars also by Cohen et al. (2004), Arnone et al. (2005), and Spite et al. (2005) and will be further discussed in the next paper of this series (Bonifacio et al., in preparation). These results are clearly inconsistent with current inhomogeneous chemical evolution models, which predict a scatter of order 1 dex for such elements (Argast et al. 2002).

As emphasized by Argast et al. (2002), the initial scatter of a given element ratio, [X/Fe], is determined by the adopted nucleosynthesis yields. The details of the chemical evolution model will then determine how fast a homogeneous ISM is achieved through mixing of the enriched regions. The results of Paper V indicated that, in order to reproduce the observed low scatter in [α/Fe], the galactic chemical evolution model must employ yields of [α/Fe] with little or no dependence on the mass of the progenitor. In homogeneous chemical evolution models (François et al. 2004), instantaneous mixing is assumed and more variation in the yield can be allowed, because it is integrated over the different stellar masses as the galaxy evolves.

As the number of EMP stars with high-resolution, high S/N spectroscopy has increased, our ability to quantify the trends and scatter about such trends for individual elements has improved dramatically as well. In such studies, it is particularly important to use data sets that are reduced and analysed in as homogeneous a manner as possible, so as to minimise the influence of spurious "observer" scatter on the behaviours that one seeks to

Table 6. Robust estimates of scatter for the observed abundance ratios (see text). "[l/Fe]" represents [⟨Sr, Y, Zr⟩/Fe].

Ord.	Abs.	N	Range	S_{BI} (CL, CU)	Ord.	Abs.	N	Range	S_{BI} (CL, CU)
[Sr/Fe]	[Fe/H]	31	≤–2.0	0.433 (0.324, 0.542)	[Sm/Fe]	[Fe/H]	8	≤–2.0	0.464 (0.293, 0.634)
		11	−2.0 to −3.0	0.244 (0.166, 0.323)					
		20	≤–3.0	0.639 (0.439, 0.838)	[Eu/Fe]	[Fe/H]	18	≤–2.0	0.306 (0.177, 0.435)
							10	−2.0 to −3.0	0.338 (0.250, 0.426)
[Y/Fe]	[Fe/H]	26	≤–2.0	0.307 (0.259, 0.354)			8	≤–3.0	0.274 (0.000, 0.551)
		11	−2.0 to −3.0	0.199 (0.155, 0.243)					
		15	≤–3.0	0.388 (0.309, 0.468)	[Gd/Fe]	[Fe/H]	14	≤–2.0	0.526 (0.407, 0.646)
							8	−2.0 to −3.0	0.449 (0.275, 0.623)
[Zr/Fe]	[Fe/H]	26	≤–2.0	0.284 (0.212, 0.356)			6	≤–3.0	0.664 (0.431, 0.896)
		11	−2.0 to −3.0	0.244 (0.166, 0.323)					
		15	≤–3.0	0.374 (0.254, 0.494)	[Dy/Fe]	[Fe/H]	13	≤–2.0	0.202 (0.052, 0.353)
							8	−2.0 to −3.0	0.145 (0.095, 0.196)
[Y/Sr]	[Fe/H]	25	≤–2.0	0.104 (0.074, 0.133)			5	≤–3.0	0.743 (0.357, 1.130)
		11	−2.0 to −3.0	0.122 (0.090, 0.154)					
		14	≤–3.0	0.083 (0.035, 0.131)	[Ho/Fe]	[Fe/H]	9	≤–2.0	0.574 (0.375, 0.774)
[Y/Sr]	[Sr/H]	25	≤–2.0	0.065 (0.051, 0.079)	[Er/Fe]	[Fe/H]	16	≤–2.0	0.299 (0.154, 0.444)
		12	−2.0 to −3.0	0.095 (0.049, 0.141)			10	−2.0 to −3.0	0.239 (0.130, 0.348)
		13	≤–3.0	0.053 (0.037, 0.070)			6	≤–3.0	0.584 (0.241, 0.926)
[l/Fe]	[Fe/H]	24	≤–2.0	0.270 (0.201, 0.338)	[Tm/Fe]	[Fe/H]	6	≤–2.0	0.398 (0.197, 0.598)
		11	−2.0 to −3.0	0.222 (0.156, 0.287)					
		13	≤–3.0	0.363 (0.234, 0.492)	[Yb/Fe]	[Fe/H]	6	≤–2.0	0.556 (0.370, 0.743)
[l/Ba]	[Ba/H]	24	≤–1.0	0.232 (0.191, 0.272)	[Eu/Ba]	[Fe/H]	18	≤–2.0	0.103 (0.081, 0.124)
		9	−2.0 to –4.0	0.198 (0.131, 0.265)			10	−2.0 to −3.0	0.121 (0.084, 0.158)
		15	≤–4.0	0.264 (0.201, 0.328)			8	≤–3.0	0.078 (0.048, 0.109)
[Ba/Fe]	[Fe/H]	30	≤–2.0	0.412 (0.324, 0.501)	[Eu/La]	[Fe/H]	15	≤–2.0	0.037 (0.011, 0.064)
		11	−2.0 to −3.0	0.413 (0.296, 0.529)			10	−2.0 to −3.0	0.045 (0.009, 0.081)
		19	≤–3.0	0.441 (0.286, 0.597)			13	≤–3.0	0.026 (0.000, 0.057)
[La/Fe]	[Fe/H]	18	≤–2.0	0.407 (0.255, 0.559)	[Sr/Ba]	[Ba/H]	29	≤–1.0	0.312 (0.264, 0.361)
		11	−2.0 to −3.0	0.409 (0.301, 0.517)			19	−2.0 to –4.0	0.290 (0.240, 0.340)
		7	≤–3.0	0.175 (0.000, 0.507)			10	≤–4.0	0.379 (0.274, 0.484)
[Ce/Fe]	[Fe/H]	13	≤–2.0	0.038 (0.000, 0.217)	[Y/Ba]	[Ba/H]	26	≤–1.0	0.200 (0.143, 0.256)
		9	−2.0 to −3.0	0.014 (0.000, 0.257)			18	−2.0 to –4.0	0.179 (0.129, 0.220)
		4	≤–3.0	0.068 (0.000, 0.187)			8	≤–4.0	0.358 (0.211, 0.506)
[Pr/Fe]	[Fe/H]	14	≤–2.0	0.285 (0.162, 0.409)	[Zr/Ba]	[Ba/H]	25	≤–1.0	0.221 (0.170, 0.272)
		10	−2.0 to −3.0	0.255 (0.169, 0.340)			19	−2.0 to –4.0	0.226 (0.177, 0.276)
		4	≤–3.0	0.168 (0.000, 0.362)			6	≤–4.0	0.124 (0.000, 0.266)
[Nd/Fe]	[Fe/H]	18	≤–2.0	0.225 (0.131, 0.319)					
		11	−2.0 to −3.0	0.229 (0.159, 0.299)					
		7	≤–3.0	0.135 (0.000, 0.376)					

understand. It was a key goal of our project to produce such data sets.

Thus, Table 6 presents estimates of the observed scatter of the elemental ratios reported here, following the order of the figures presenting the information, but based exclusively on the stars analysed by ourselves. The first two columns in the table present the ordinates and abscissae corresponding to each of the figures. The number of stars considered in each range of abscissae listed in the table appears in the third column, while the range in the parameter under discussion is listed in the fourth column.

In order to obtain robust estimates of scatter, we must first de-trend the distributions of the observed ratios. This is accomplished by determination of robust locally weighted regression lines (*loess* lines), as described by Cleveland (1979, 1994). Such lines have been used before in similar scatter analyses (see, e.g., Ryan et al. 1996; Carretta et al. 2002). The scatter about these lines is then estimated by application of the biweight estimator of scale, S_{BI}, described by Beers et al. (1990)[1].

The first entry in the last column of Table 6 lists this estimate. The quantities in parentheses in this column are the $1-\sigma$ confidence intervals on this estimate of scatter, obtained from analysis of 1000 bootstrap resamplings of the data in each of the given ranges. In this listing, CL represents the lower interval on the value of the scatter, while UL represents the upper interval. These errors are useful for assessing the significance of the difference between the scales of the data from one range to another.

[Sr/Fe], [Y/Fe], and [Zr/Fe] shows a similar increase of the scatter as the metallicity decreases, with a more pronounced

[1] The scale matches the dispersion for a normal distribution.

effect for Sr. The mean ratio [⟨Sr + Y + Zr⟩/Fe] shows the same behaviour with a lower amplitude.

Large scatter is also seen in Ba and La, but its variation as a function of metallicity differs from the lighter elements. The dispersion found for Ba seems independent of metallicity, whereas the scatter of La appears much smaller for the most metal-poor stars. Ce, Pr and Nd show much smaller scatter again, in particular Ce for which we measure a bi-weight estimator of only 0.038 dex for the whole sample. Pr and Nd behave like La with smaller scatter for the most metal-poor stars.

Eu shows a rather high scatter, decreasing as the metallicity decreases. In contrast, Gd, Dy and Er follow the same behaviour as Sr, i.e. an increase in scatter as the metallicity decreases.

If we now consider the ratios [Eu/Ba] and [Eu/La] as a function of [Fe/H], the scatter is smaller by almost an order of magnitude, confirming the common origin of these elements. It is also noteworthy that the scatter is even smaller for the most metal poor metallicity bin.

5.4. Abundance scatter and inhomogeneous models of galactic chemical evolution

The apparently contradictory abundance results for the α- and various neutron-capture elements in VMP and EMP stars might be reconciled if the sites of significant *r*-process production were diverse and (some of them) rare. And we caution that r-II stars *are* rare: Barklem et al. (2005) estimate that they constitute roughly 5% of the giants with [Fe/H] < -2.0. The lower probability of finding them at metallicities below [Fe/H] $\simeq -3.20$ may introduce an artificial decrease of the observed scatter.

The highly *r*-enriched (r-II) stars have all been found in a very narrow range around [Fe/H] = −2.9 (Barklem et al. 2005). Do we see the onset of a new process at this metallicity? Does this metallicity correspond to the typical metallicity of the building blocks of the halo, originating from systems of similar size (i.e. about the same metallicity) but with different chemical histories (IMF, fraction of peculiar supernovae), leading to a spread of [n-capture/Fe] but keeping an *r*-process signature. Did the stars with [Fe/H] < -3.5 form out of matter polluted by massive Pop III stars, which could mean that they are pre-galactic?

It is interesting to note how difficult it has been to find true UMP stars, i.e. stars with [Fe/H] < -4; in fact, only three are currently known (Christlieb et al. 2002; Frebel et al. 2005; Norris et al. 2007). In a standard closed-box model (François et al. 1990), we would expect to have found several more, if the IMF did not change substantially over time; however, the preferred scheme for the halo formation is an open model, where infall is invoked to explain this "UMP desert" (Chiappini et al. 1997).

In the context of an inhomogeneous model of chemical evolution of the Galaxy (Argast et al. 2002), simulations show that the density of stars at [Fe/H] = −3.0 and [Fe/H] = −4.0 is of the same order (Argast et al. 2002, see their Fig. 7). As a consequence, the paucity of UMP stars would require rather fine tuning of the mixing of supernovae ejecta into the ISM. However, Karlsson (2006) has suggested that, alternatively, the absence of UMP stars could be explained with a galactic chemical evolution model where star formation was low or delayed for a period after the formation and demise of the first generation of stars, due to heating of the ISM by their supernova explosions.

Another possibility is that stars in the inner and outer regions of the halo of the Milky Way may have rather different metallicity distribution functions (MDFs). From a kinematic analysis of a local sample of stars from the Sloan Digital Sky Survey, Carollo et al. (2007) argue that just such a dichotomy exists, with the MDF of the inner-halo stars peaking around [Fe/H] = −1.6, that of the outer halo around [Fe/H] = −2.2.

The magnitude-limited objective-prism surveys that have identified the most metal-poor halo stars to date may thus have been dominated by inner-halo objects. If so, simple models of Galactic chemical evolution that match the MDFs derived from such surveys may not provide adequate explanations for the formation of the Milky Way halo, nor for the detailed chemical composition of its most primitive stars.

6. Conclusions

This paper has presented accurate, homogeneous abundance determinations for 16 neutron-capture elements in a sample of 32 VMP and EMP giant stars, for which abundances of the lighter elements have been determined earlier (Paper V). Our data confirm and refine the general results of earlier studies of the neutron-capture elements in EMP stars, and extend them to lower metallicities. In particular, the sample of stars below [Fe/H] = −2.8 is increased significantly.

Our data show the [n-capture/Fe] ratios, and their scatter around the mean value, to reach a maximum around [Fe/H] $\simeq$ −3.0. Below [Fe/H] $\simeq -3.2$, we do not find stars with large overabundances of neutron-capture elements relative to the solar ratio. We note, however, that the large "snapshot" sample of Barklem et al. (2005) does identify at least a few stars below [Fe/H] = −3.0 with high [Sr/Fe], [Zr/Fe], or [Eu/Fe], so a larger sample of accurate data may be needed for a firm conclusion.

Adopting Ba as a reference element in the abundance ratios reveals very tight anti-correlations of [Sr/Ba], [Y/Ba] and [Zr/Ba] ratios with [Ba/H] abundance from [Ba/H] $\simeq -1.5$ down to [Ba/H] $\simeq -4.5$.These results confirm the need for a second neutron-capture process for the synthesis of the first-peak elements, called the "weak" *r*-process (Busso et al. 1999; Qian & Wasserburg 2000; Wanajo et al. 2001), LEPP process (Travaglio et al. 2004), or CPR process (Qian & Wasserburg 2007), or even an entirely new nucleosynthesis mechanism in massive, metal-poor stars (νp-process, Froehlich et al. (2006). By subtracting the contributions of the main *r*-process, we show that this mechanism is responsible for 90–95% of the amounts of Sr, Y, and Zr in stars with [Ba/H] > -4.5. Below this value, the [Sr/Ba], [Y/Ba], and [Zr/Ba] ratios seem to return to the solar ratio, although the number of stars in this range is small.

As found earlier (Ryan et al. 1996; McWilliam 1998; Honda et al. 2004), the [n-capture/Fe] ratios exhibit a much larger dispersion than can be attributed to observational errors, although the scatter in their [α/Fe] and [Fe-peak/Fe] ratios as functions of [Fe/H] is very small. We discuss the implications of these apparently contradictory results on the efficiency of mixing of the primitive ISM in terms of homogeneous vs. inhomogeneous models of galactic chemical evolution.

Acknowledgements. We thank the ESO staff for assistance during all the runs of our Large Programme. R.C., P.F., V.H., B.P., F.S. & M.S. thank the PNPS and the PNG for their support. PB and PM acknowledge support from the MIUR/PRIN 2004025729_002 and PB from EU contract MEXT-CT-2004-014265 (CIFIST). T.C.B. acknowledges partial funding for this work from grants AST 00-98508, AST 00-98549, and AST 04-06784 as well as from grant PHY 02-16783: Physics Frontiers Center/Joint Institute for Nuclear Astrophysics (JINA), all awarded by the US National Science Foundation. B.N. and J.A. thank the Carlsberg Foundation and the Swedish and Danish Natural Science Research Councils for partial financial support of this research.

References

Abel, T., Bryan, G. L., & Norman, M. L. 2000, ApJ, 540, 39
Alonso, A., Arribas, S., & Martínez-Roger, C. 1998, A&AS, 131, 209
Alonso, A., Arribas, S., & Martinez-Roger, C. 1999, A&AS, 140, 261
Alvarez, R., & Plez, B. 1998, A&A, 330, 1109
Arlandini, C., Käppeler, F., Wisshak, K., et al. 1999, ApJ, 525, 886
Argast, D., Samland, M., Thielemann, F.-K., & Gerhard, O. E. 2002, A&A, 388, 842
Arnone, E., Ryan, S. G., Argast, D., Norris, J. E., & Beers, T. C. 2005, A&A, 430, 507
Asplund, M., Gustafsson, B., Kiselman, D., & Eriksson, K. 1997, A&A, 318, 521
Barklem, P. S., Christlieb, N., Beers, T. C., et al. 2005, A&A, 439, 129
Beers, T. C., & Christlieb, N. 2005, ARA&A, 43, 531
Beers, T. C., Preston, G. W., & Schectman, S. A. 1985, AJ, 90, 2089
Beers, T. C., Flynn, C., & Gebhardt, K. 1990, AJ, 100, 32
Bromm, V. 2005, in From Lithium to Uranium, ed. V. Hill, P. François, & F. Primas, IAU Symp., 228, 121
Burstein, D., & Heiles, C. 1982, AJ, 87, 1165
Burris, D. L., Pilachowski, C. A., Armandroff, T. E., et al. 2000, ApJ, 544, 302
Busso, M., Gallino, R., & Wasserburg, G. J. 1999, ARA&A, 37, 239
Carney, B. W., Wright, J. S., Sneden, C., et al. 1997, AJ, 114, 363
Carollo, D., Beers, T. C., Lee, Y. S., et al. 2007, Nature, submitted [arXiv:0706.3005v2]
Carretta, E., Gratton, R., Cohen, J. G., Beers, T. C., & Christlieb, N. 2002, AJ, 124, 481
Cayrel, R., Depagne, E., Spite, M., et al. 2004, A&A, 416, 1117 (Paper V)
Cescutti, G., François, P., Matteucci, F., Cayrel, R., & Spite, M. 2005, A&A, 448, 557
Charbonneau, P. 1995, ApJS, 101, 309
Chiappini, C., Matteucci, F., & Gratton, R. 1997, ApJ, 77, 765
Christlieb, N., Bessell, M., Beers, T. C., et al. 2002, Nature, 419, 904
Christlieb, N., Beers, T. C., Barklem, P. S., et al. 2004, A&A, 428, 1027
Cleveland, W. S. 1979, J. Am. Stat. Assoc., 74, 829
Cleveland, W. S. 1984, The Elements of Graphing Data, rev. ed., Summit, NJ: Hobart
Cohen, J. G., Christlieb, N., McWilliam, A., et al. 2004, ApJ, 612, 1107
Dekker, H., D'Odorico, S., Kaufer, A., Delabre, B., & Kotzlowski 2000, in Optical and IR Telescope Instrumentation and Detectors, ed. M. Iye, & A. F. Moorwood, Proc SPIE, 4008, 534
Den Hartog, E. A., Lawler, J. E., Sneden, C., & Cowan, J. J. 2003, ApJS, 148, 543
Edvardsson, B., Andersen, J., Gustafsson, B., et al. 1993, A&A, 275, 101
François, P., Vangioni-Flam, E., & Audouze, J. 1990 ApJ, 361, 487
François, P., Matteucci, F., Cayrel, R., et al. 2004, A&A, 421, 613
Frebel, A., Aoki, W., Christlieb, N., et al. 2005, Nature, 434, 871
Frebel, A., Christlieb, N., Norris, J. E., et al. 2007, ApJ, 660, L117
Fröhlich, C., Martinez-Pinedo, G., Liebendörfer, M., et al. 2006, Phys. Rev. Lett., 96, 142502
Fulbright, J. P. 2000, AJ, 120, 1841
Fuller, T. M., & Couchman, H. M. P. 2000, ApJ, 544, 6
Gilroy, K. K., Sneden, C., Pilachowski, C. A., & Cowan, J. J. 1988, ApJ, 327, 298
Goriely, S., & Arnould, M. 1997, A&A, 322, 29
Gratton, R. G. 1989, A&A, 208, 171
Gratton, R. G., & Sneden, C. 1987, A&A, 178, 179
Gratton, R. G., & Sneden, C. 1988, A&A, 204, 193
Gratton, R. G., & Sneden, C. 1991, A&A, 241, 501
Gratton, R. G., & Sneden, C. 1994, A&A, 287, 927
Grevesse, N., & Sauval, A. J. 2000, Origin of Elements in the Solar System, ed. O. Manuel, 261
Gustafsson, B., Bell, R. A., Eriksson, K., & Nordlund, Å. 1975, A&A, 42, 407
Gustafsson, B., Edvardsson, B., Eriksson, K., et al. 2003, in Stellar Atmosphere Modeling, ed. I. Hubeny, D. Mihalas, & K. Werner, ASP Conf. Ser., 288, 331
Hill, V., Plez, B., Cayrel, R., et al. 2002, A&A, 387, 560 (Paper I)
Honda, S., Aoki, W., Ando, H., et al. 2004, ApJS, 152, 113
Johnson, J. A., & Bolte, M. 2002, ApJ, 579, 616
Karlsson, T. 2006, ApJ, 641, L41
Ishimaru, Y., & Wanajo, S. 1999, ApJ, 511, L33
Ishimaru, Y., & Wanajo, S. 2000, The First Stars, ed. A. Weiss, T. Abel, & V. Hill (Springer), 189
Ishimaru, Y., Wanajo, S., Aoki, W., & Ryan, S. G. 2004, ApJ, 600, 47
Lawler, J. E., Sneden, C., & Cowan, J. J. 2004, ApJ, 604, 850
Lucatello, S., Tsangarides, S., Beers, T. C., et al. 2005, ApJ, 625, 825
Madau, P., Rees, M. J., Volonteri, M., Haardt, F., & Oh, S. P. 2004, ApJ, 604, 484
McWilliam, A. 1998 AJ, 115, 1640
McWilliam, A., Preston, G. W., Sneden, C., & Searle, L. 1995, AJ, 109, 2757
Molaro, P., & Bonifacio, P. 1990, A&A, 236, L5
Nissen, P. E., & Schuster, W. J. 1997, A&A, 326, 751
Norris, J. E., Peterson, R. C., & Beers, T. C. 1993, ApJ, 415, 797
Norris, J. E., Ryan, S. G., & Beers, T. C. 2001, ApJ, 561, 1034
Norris, J., et al. 2007, ApJ, submitted
Plez, B., Brett, J. M., & Nordlund, Å. 1992, A&A, 256, 551
Prantzos, N., Hashimoto, M., & Nomoto, K. 1990, A&A, 234, 211
Primas, F., Molaro, P., & Castelli, F. 1994, A&A, 290, 885
Qian Y. Z., & Wasserburg, G. J. 2000, Phys. Rep., 333, 77
Qian, Y. Z., & Wasserburg, G. J. 2007, Phys. Rep., 444, 237
Ryan, S. G., Norris, J. E., & Bessell, M. S. 1991, AJ, 102, 303
Ryan, S. G., Norris, J. E., & Beers, T. C. 1996, ApJ, 471, 254
Schlegel, D. J., Finkbeiner, D. P., & Davis, M. 1998, ApJ, 500, 525
Sivarani, T., Beers, T. C., Bonifacio, P., et al. 2006, A&A, 459, 125 (Paper X)
Sneden, C., McWilliam, A., Preston, G. W., et al. 1996, ApJ, 467, 819
Spite, M. 1967, Ann. Astrophys., 30, 211
Spite, M., & Spite, F. 1978, A&A, 67, 23
Spite, M., Bonifacio, P., Cayrel, R., et al. 2005, in ed. V. Hill, P. François, & F. Primas (Cambridge Univ. Press), IAU Symp., 228, 185
Stephens, A. 1999, AJ, 117, 1771
Travaglio, C., Gallino, R., Arnone, E., et al. 2004, ApJ, 601, 864
Truran, J. W. 1981, A&A, 97, 391
Wanajo, S., Kajino, T., Mathews, G. J., & Otsuki, K. 2001, ApJ, 554, 578
Woosley, S. E., & Hoffmann, R. D. 1992, ApJ, 395, 202
Yoshida, N., Sokasian, A., Hernquist, L., & Springel, V. 2003, ApJ, 598, 73